



Citation for published version:

Sayers, C, Farrar, L, Bending, S, Cattelan, M, Jones, A, Fox, N, Kociok-Kohn, G, Koshmak, K, Laverock, J, Pasquali, L & Da Como, E 2020, 'Correlation between crystal purity and the charge density wave in 1T-VSe₂', *Physical Review Materials*, vol. 4, 025002. <https://doi.org/10.1103/PhysRevMaterials.4.025002>

DOI:

[10.1103/PhysRevMaterials.4.025002](https://doi.org/10.1103/PhysRevMaterials.4.025002)

Publication date:

2020

Document Version

Peer reviewed version

[Link to publication](#)

(C) 2020 American Physical Society

University of Bath

General rights

Copyright and moral rights for the publications made accessible in the public portal are retained by the authors and/or other copyright owners and it is a condition of accessing publications that users recognise and abide by the legal requirements associated with these rights.

Take down policy

If you believe that this document breaches copyright please contact us providing details, and we will remove access to the work immediately and investigate your claim.

Correlation between crystal purity and the charge density wave in 1T-VSe₂

C. J. Sayers,^{1,*} L. S. Farrar,¹ S. J. Bending,¹ M. Cattelan,² A. J. H. Jones,³ N. A. Fox,^{2,3}
G. Kociok-Köhn,⁴ K. Koshmak,⁵ J. Laverock,³ L. Pasquali,^{5,6,7} and E. Da Como¹

¹*Centre for Nanoscience and Nanotechnology, Department of Physics, University of Bath, Bath, BA2 7AY, UK*

²*School of Chemistry, University of Bristol, Cantocks Close, Bristol BS8 1TS, UK*

³*HH Wills Physics Laboratory, University of Bristol, Tyndall Avenue, Bristol BS8 1TL, UK*

⁴*Material and Chemical Characterisation Facility (MC²),
University of Bath, Claverton Down, Bath BA2 7AY, UK*

⁵*IOM-CNR Institute, Area Science Park, SS 14 Km, 163.5, Basovizza, 34149 Trieste, Italy*

⁶*Dipartimento di Ingegneria “Enzo Ferrari”, Università di Modena e Reggio Emilia, via P. Vivarelli 10, 41125 Modena, Italy*

⁷*Department of Physics, University of Johannesburg,
P.O. Box 524, Auckland Park 2006, South Africa*

We examine the charge density wave (CDW) properties of 1T-VSe₂ crystals grown by chemical vapour transport (CVT) under varying conditions. Specifically, we find that by lowering the growth temperature ($T_g < 630^\circ\text{C}$), there is a significant increase in both the CDW transition temperature and the residual resistance ratio (RRR) obtained from electrical transport measurements. Using x-ray photoelectron spectroscopy (XPS), we correlate the observed CDW properties with stoichiometry and the nature of defects. In addition, we have optimized a method to grow ultra-high purity 1T-VSe₂ crystals with a CDW transition temperature, $T_{\text{CDW}} = (112.7 \pm 0.8)$ K and maximum residual resistance ratio (RRR) ≈ 49 , which is the highest reported thus far. This work highlights the sensitivity of the CDW in 1T-VSe₂ to defects and overall stoichiometry, and the importance of controlling the crystal growth conditions of strongly-correlated transition metal dichalcogenides.

I. INTRODUCTION

The metallic transition metal dichalcogenides (TMDs) are well-known to exhibit interesting strongly correlated behaviour such as charge density waves (CDWs) [1, 2] and superconductivity. In 1T-VSe₂, an incommensurate CDW develops at $T_{\text{CDW}} = 110$ K with $(4a \times 4a \times 3.18c)$ periodic lattice distortion, followed by a further change in the distorted c -axis to $3.25c$ below 85 K [3]. Signatures of these phase transitions have been noted in x-ray [3] and electron diffraction [4], magnetic and transport studies [5]. The CDW is likely driven by Fermi surface nesting involving states along the flat portions of the electron pocket centred around the \bar{M} -point at the edge of the Brillouin zone [6], which possibly has a three-dimensional character [7]. The common polytype of VSe₂ has the trigonal (1T) unit cell and belongs to the $P\bar{3}m1$ spacegroup [4]. Fig. 1(a) and (b) shows the layered structure consisting of Se-V-Se planes in the a - b direction separated by a van der Waals (vdW) gap, and octahedral metal coordination when viewed along the c -axis.

In addition to the ongoing efforts to understand CDW transitions in bulk TMDs, the recent surge in research of layered 2D materials has reignited interest in this area. So far, it has been shown that 1T-VSe₂ has a large range of tunability of its CDW properties with dimensionality, as the transition temperature and magnitude of the order parameter are strongly influenced by the sample thickness on a nanometre scale [8, 9]. Control of the distorted lattice periodicity is also possible by strain engineering,

and an unconventional $(4a \times \sqrt{3}a)$ CDW has been observed by STM [19]. At the monolayer limit, there have been reports of possible ferromagnetism [10–12], strongly enhanced CDW order evidenced by a fully-gapped Fermi surface [13], and an increase of the transition temperature up to $T_{\text{CDW}} = 220$ K [14].

With increasing interest in studying monolayer or few-layer charge density wave TMDs, the bottom-up approach of growth by molecular beam epitaxy (MBE) [13, 19] or chemical vapour deposition (CVD) [15, 16] techniques has become common. Once optimized, these methods are excellent at producing thin films. However, samples produced this way often suffer from a high number of crystal defects. In particular, the presence of grain boundaries due to coalescing nucleation sites is a common and well-documented problem in 2D materials grown by CVD, such as graphene [17]. Also, there is often an unavoidable interaction with the growth substrate such as doping [18] or strain [19] which can alter the sample properties. Instead, a top-down approach by exfoliation of high-quality crystals as the starting material is still considered the ideal way to obtain pristine monolayers and to provide the basis for construction of van der Waals heterostructures by dry transfer [20].

At present, many researchers either grow their own crystals or obtain them commercially. In both cases, the specific growth conditions are often not reported. However, notably among the TMDs, 1T-VSe₂ can grow far from ideal stoichiometry in varying conditions [21]. Previous investigations on 1T-VSe₂ have suggested that the CDW transition temperature is maximum for samples prepared using the lowest growth temperatures ($T_g < 600^\circ\text{C}$) where the Se:V ratio is expected to approach 2:1 [22, 23]. Deviations from ideal stoichiometry due to in-

*Corresponding author: c.j.sayers@bath.ac.uk

creasing density of defects can occur at higher growth temperatures, but their nature in this compound remains unknown. Types of defects that are typically found in TMD crystals are labelled in Fig. 1(a) and (b) including vacancies and interstitials [24]. The influence of growth temperature on crystal purity and its relation to CDW properties has been reported in the related compound $1T$ -TiSe₂. Increasing Ti interstitials in the vdW gap between the layers results in electron doping and reduces T_{CDW} by upsetting the delicate balance of electrons to holes which has consequences within the excitonic insulator scenario [25]. In $1T$ -VSe₂, where Fermi surface nesting is suggested to play a role, such a doping effect could have a significant impact on the CDW by altering the topology of the Fermi surface due to the change in chemical potential. Thus far, a detailed study of the growth conditions of $1T$ -VSe₂ in relation to its CDW properties and the role of defects is lacking.

Here, we show that changes in the growth temperature over the range (550 - 700)°C have a significant impact on the physical purity, structure, and intrinsic stoichiometry which subsequently influences the CDW behaviour. Electronic transport measurements show that the CDW transition temperature increases markedly for crystals grown with $T_{\text{g}} < 630^\circ\text{C}$. Using x-ray spectroscopy, we are able to identify defects in samples grown at higher temperatures, and correlate this with the observed electronic properties. In addition, we have optimized the conditions for growing ultra-pure $1T$ -VSe₂ at $T_{\text{g}} = 550^\circ\text{C}$ with a transition temperature of $T_{\text{CDW}} = (112.7 \pm 0.8)$ K and a maximum residual resistance ratio (RRR) ≈ 49 which, to the best of our knowledge, surpasses the highest value reported previously of ~ 28 [26, 27].

II. EXPERIMENTAL METHODS

A. Crystal growth

$1T$ -VSe₂ crystals were grown using a chemical vapour transport (CVT) method [28], whereby a constant temperature gradient drives the crystallisation of the elements from a vapour at high temperature as illustrated in Fig. 1(d). High purity vanadium (99.9%) and selenium (99.99%) powders were sealed inside an evacuated quartz ampoule, together with anhydrous iodine (99.998%) which acts as the transport agent. Under inert atmosphere (N₂ glovebox), stoichiometric amounts of the elements (2:1 molar ratio) were loaded plus a slight excess of selenium (2.4 - 3.4 mg cm⁻³), based on the ampoule volume. The amount of iodine (2.10 - 2.25 mg cm⁻³) was chosen to facilitate growth within a reasonable time-frame [29], whilst also minimizing the potential for iodine to be introduced into the crystals which is known to suppress the CDW transition in other TMDs [25]. The ampoule was evacuated using a pump capable of achieving base pressure (7×10^{-6}) mbar and then sealed with a flame. A two-zone tube furnace was used with

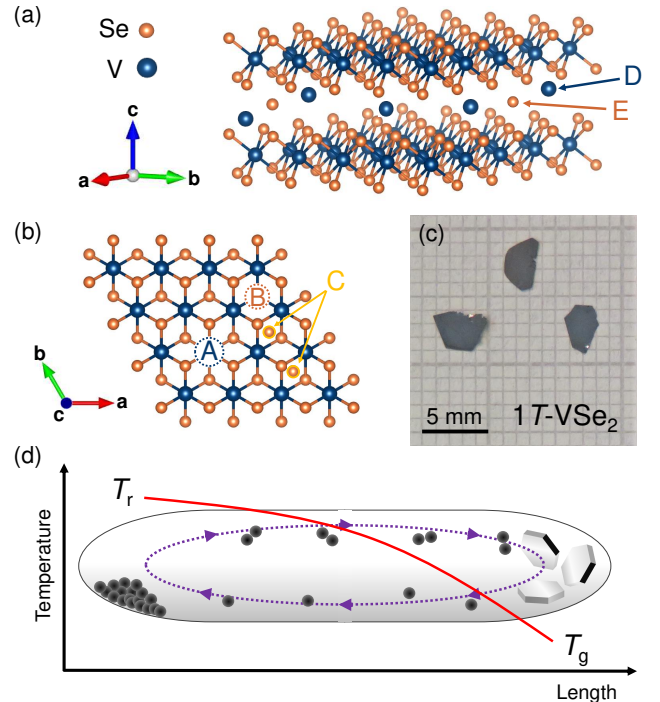


FIG. 1: Growth of $1T$ -VSe₂ crystals. Panels (a) and (b) show the crystal structure of $1T$ -VSe₂ viewed along the layer plane and c -axis respectively. Common defect types found in TMDs are labelled. In $1T$ -VSe₂, these correspond to vanadium and selenium vacancies (A and B), selenium aggregates/clusters (C), and interstitials in the van der Waals (vdW) gap between the layer planes (D and E). (c) Image of typical crystals produced by CVT (d) Illustration of the chemical vapour transport (CVT) process. Iodine vapour carries material from the reaction zone at T_r to the growth zone at T_g where crystals form. The solid red line is a sketch of a typical temperature profile.

a temperature gradient between hot (reaction temperature, T_r) and cold (growth temperature, T_g) zones of $\Delta T = (55 - 60)^\circ\text{C}$ which was confirmed with a thermocouple probe. The temperature stability was better than $\pm 1^\circ\text{C}$. Growth proceeded for up to 21 days, resulting in many crystals of (5 x 5 x 0.1 mm) forming at the cold end of the ampoule. The crystals were typically thin platelets with hexagonal edges and a highly reflective silver appearance as shown in Fig. 1(c).

With these general conditions, this procedure was carried out several times in order to produce separate sample batches with different growth temperatures, T_g in the range (550 - 700)°C.

B. Electronic transport

We measured the resistance as a function of temperature, $R(T)$ for different crystal batches. Samples were cut with a razor blade into rectangular shapes (typical lateral size 4 mm x 1 mm) and mounted on electrically insulating substrates using thermal varnish. Contacts

were made to the as-grown crystal surfaces using silver paste in a standard 4-point configuration. Measurements were performed in a JANIS 4 K closed cycle cryocooler (4 - 300 K) using a lock-in amplifier (SR830) and a typical excitation current of 1 mA.

Multiple crystals were measured from each batch to investigate any possible variations.

C. X-ray spectroscopy

We used both x-ray photoelectron spectroscopy (XPS) and x-ray absorption spectroscopy (XAS) with synchrotron radiation to study core levels of selenium (Se), vanadium (V) and iodine (I) in $1T$ -VSe₂. Measurements were performed at the BEAR end station (Elettra synchrotron, Trieste) [30, 31]. In order to expose a clean surface, the samples were cleaved in a nitrogen glove-bag attached to the fast entry of the preparation chamber.

We found that after prolonged exposure, we were able to induce radiation damage to the sample surface which resulted in noticeable changes in the spectra. Hence, for the results presented in the main text and the Supplemental Material (Ref. [32]), we minimized both the exposure time and photon flux (e.g. $\sim 7 \times 10^{10}$ photons s^{-1} at $h\nu = 150$ eV). Identical experimental conditions were maintained for each sample. As a result of these measures, we did not observe any evolution of the spectra during the measurements which could be related to damage and therefore the properties we report are intrinsic to the samples.

III. ELECTRONIC PROPERTIES

To investigate the bulk electronic properties of $1T$ -VSe₂, we measured the resistance as a function of temperature, $R(T)$ for different crystal batches as shown in Fig. 2(a). The shape of the curve agrees with previous studies of $1T$ -VSe₂ and shows an overall metallic behaviour with a slight increase in the resistance related to the CDW transition at $T_{CDW} \approx (100 - 110)$ K [5, 33, 34]. At low temperature, the resistivity approaches a finite value related to the amount of impurity scattering [33]. We do not see any indication of an upturn in the resistance of our samples at low temperature (4 K) in contrast to a previous study, which attributed this behaviour to a Kondo effect [35].

The first derivative, dR/dT in Fig. 2(b) highlights the CDW transition, T_{CDW} which we define as the onset temperature where the resistance first starts to increase, and corresponds to the point at which dR/dT initially crosses zero [dashed horizontal line in Fig. 2(b)]. Details of obtaining T_{CDW} in this way are provided in Ref. [32], and we emphasize that by using alternative points in dR/dT to define T_{CDW} does not change the observed trend between samples or the conclusions of

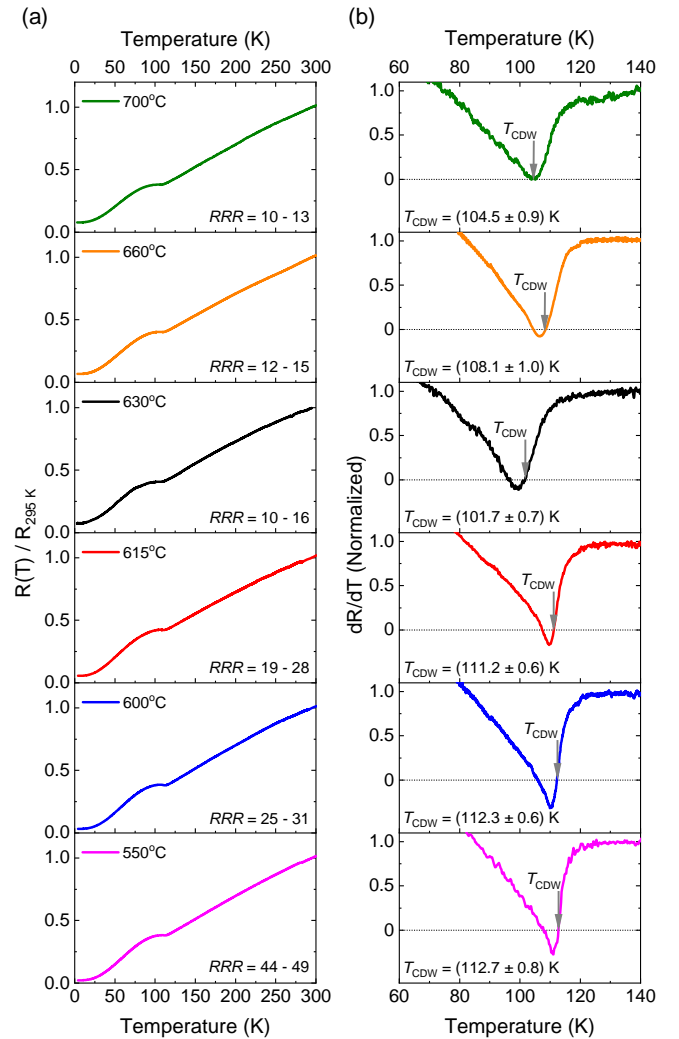


FIG. 2: Resistance of $1T$ -VSe₂ samples produced with different growth temperatures as indicated. (a) Normalized resistance, R/R_{295K} for different sample batches. The range of residual resistance ratio (RRR) for each crystal batch is labelled. (b) First derivative of resistance, dR/dT highlighting the charge density wave transition, T_{CDW} which we define as the point at which dR/dT initially crosses zero indicated by the arrows.

this work. Fig. 3(a) shows the CDW transition temperatures extracted from dR/dT for different sample batches as a function of growth temperature. The overall trend shows that T_{CDW} is increased at lower growth temperatures, reaching a maximum of $T_{CDW} = (112.7 \pm 0.8)$ K for the 550°C sample. We note that samples with $T_g < 630^\circ\text{C}$ show an increase in transition temperature above the typically reported value of $T_{CDW} = 110$ K. Based on the trend of our samples produced at the lowest growth temperatures, it seems as if T_{CDW} is approaching the inherent maximum for $1T$ -VSe₂. It is also apparent in Fig. 2(b) that there is an evolution in the width of dR/dT feature relating to the CDW transition, where there is a broadening at higher growth temperatures.

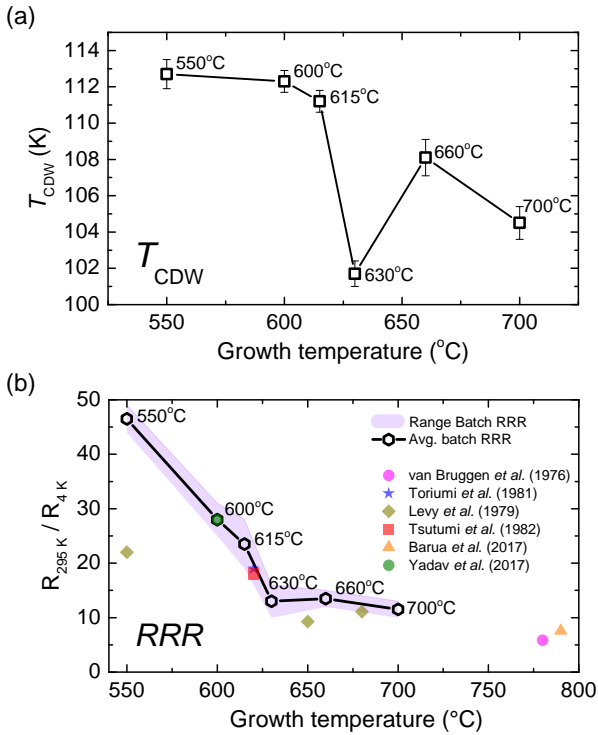


FIG. 3: Electronic properties of $1T$ -VSe₂ samples as a function of crystal growth temperature, T_g (a) Charge density wave transition temperature, T_{CDW} . (b) Average residual resistance ratio (RRR), R_{295K}/R_{4K} . The shaded area corresponds to the RRR range found within each batch of crystals. For comparison, the coloured data points show RRR values taken from the literature as indicated. If the value was not directly quoted in those works, it has been estimated here from the published resistance/resistivity data.

This is seen in both the onset of the transition (gradient of the steep decline near T_{CDW}) and width of the minima in dR/dT . Such a broadening is often linked to disorder, and the behaviour in our samples is similar to that observed in NbSe₂ using electron irradiation dosing to induce atomic defects without doping the system [37]. Additional information can be extracted from the magnitude of the dR/dT minima below zero (dashed horizontal line) which also follows a similar trend, as dR/dT of the sample with highest T_{CDW} becomes the most negative following the CDW transition. We show in Ref. [32] that this corresponds to the magnitude of the resistance increase at T_{CDW} relative to the normal metallic behaviour. Therefore our results are fully consistent with strengthened CDW order where one would expect a more effective gapping of the Fermi surface, as the proportion of charge carriers removed at T_{CDW} is greater.

The residual resistance ratio (RRR) is a well-known parameter often used to estimate the purity of metals. At sufficiently low temperatures, the scattering of carriers is dominated by impurities or crystal defects, which gives rise to a finite (residual) resistance. The magnitude

of this residual resistance is thus linked to the density of impurities and/or defects present in the sample. Using the ratio R_{295K}/R_{4K} , we are able to compare several samples as shown in Fig. 3(b). Overall, we find that the average RRR within each batch increases for lower growth temperatures, indicating a reduction in impurity/defect scattering. For samples grown at the lowest temperature (550°C), we find a maximum RRR of ~ 49 within the batch. Similar to the behaviour of the CDW transition temperature, there is also a significant increase in the average RRR from ~ 12 to > 22 for samples with $T_g < 630^\circ\text{C}$. This is consistent with the width of the CDW transitions in dR/dT [Fig. 2(b)] for samples $T_g = (630 - 700)^\circ\text{C}$, confirming a defect-induced broadening. By comparing our results to reports of RRR in the literature on $1T$ -VSe₂ over a range of growth temperatures, there is a clear agreement with this trend [Fig. 3(b)].

Finally, we discuss the scattering mechanism of charge carriers at low temperature by analyzing the temperature dependence of the resistance. Previously in $1T$ -VSe₂, there have been reports of a strong T^2 dependence [5, 34] which could suggest a significant electron-electron scattering. By fitting the low temperature data in the range (5 - 15) K with a power law, $R \propto T^x$ we also find a T^2 dependence but only for the sample grown at the highest temperature (700°C). By contrast, the sample grown at the lowest temperature (550°C) shows a T^3 behaviour, and there appears to be a progressive shift between these two regimes for intermediate temperatures (see Ref. [32]). In other CDW-bearing TMDs, a temperature dependence in the range $T^3 - T^5$ is found for $T \leq 25$ K, depending on the compound, and is related to electron-phonon scattering [36]. The power then depends on the orbital character of bands involved in either an *intra*band or *inter*band scattering, the density of states, and strength of the CDW order (proportion of carriers lost from the Fermi surface). For example, a T^3 dependence is found for the ideal resistivity in $2H$ -NbSe₂ and can be understood by a simple two-band model which describes an electron-phonon mediated *inter*band scattering of *s*-like electrons into the *d*-band. Such a two-band analysis has also been used to successfully describe the temperature dependence of the Hall coefficient in $1T$ -VSe₂ [27] and the ideal resistivity was found to be in the range $T^3 - T^4$ for the highest purity samples.

We therefore suggest that a similar electron-phonon scattering mechanism is the case for pure $1T$ -VSe₂ which is seen here in our sample with largest RRR (550°C). Instead, the low temperature resistance deviates rapidly from this behaviour with increasing disorder and approaches a T^2 dependence. Clearly, this behaviour seems to be rather sample dependent and could explain the large variation reported in the literature [5, 26, 27, 34]

In summary, the electronic properties of $1T$ -VSe₂ and its CDW behaviour vary quite significantly with crystal growth temperature. The observed trend of T_{CDW} and RRR in Fig. 3 are similar and therefore, the underlying mechanism influencing both of these properties is likely

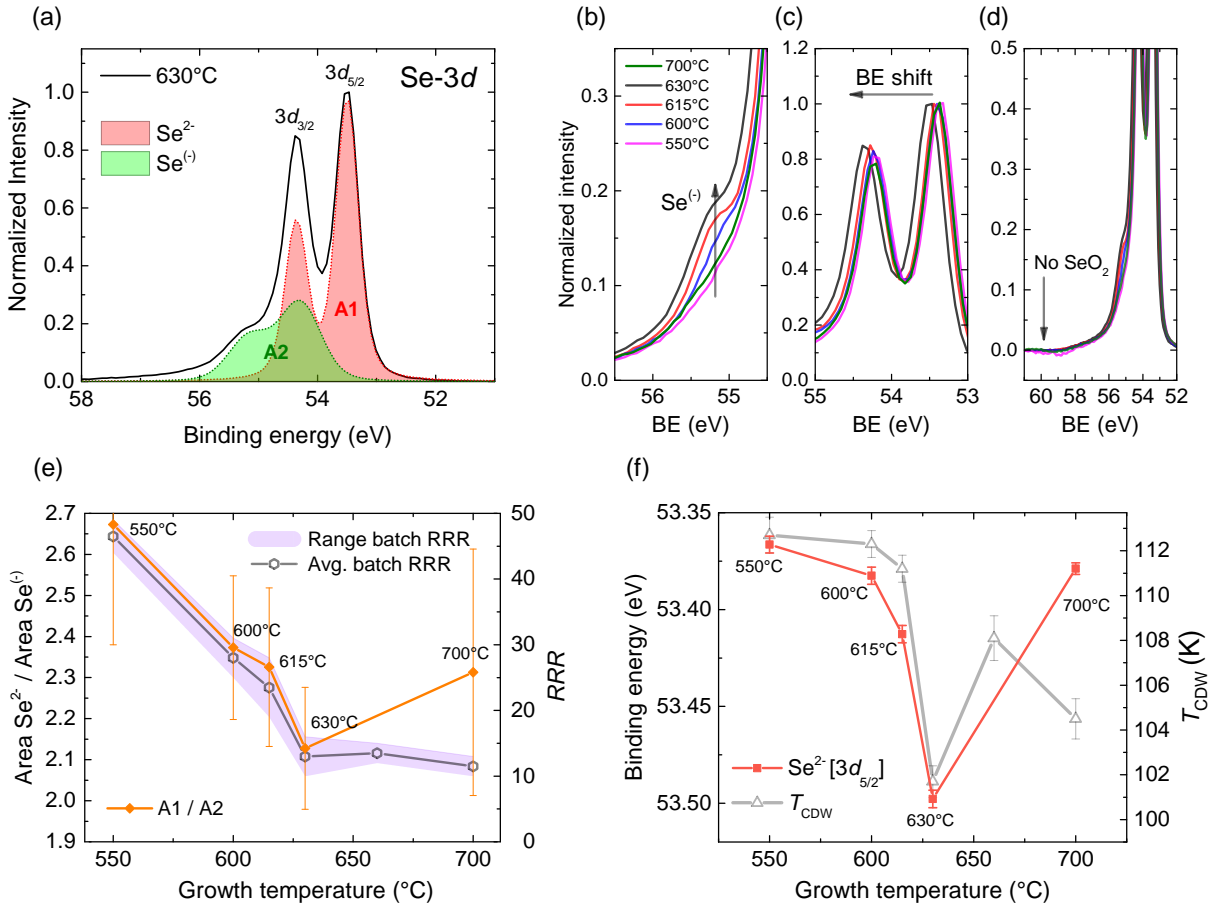


FIG. 4: X-ray photoelectron spectroscopy (XPS) of $1T$ -VSe $_2$ samples grown at different temperatures. (a) Se- $3d$ spectra ($h\nu = 150$ eV). The shaded curves are fits to the data for the $T_g = 630^\circ\text{C}$ sample, showing the contribution from Se^{2-} and $\text{Se}^{(-)}$ oxidation states. Panels (b) - (d) show the same data as panel (a) and highlight the feature in Se- $3d$ spectra related to the presence of $\text{Se}^{(-)}$, the observed shift in binding energy (BE), and the absence of SeO_2 . (e) The area ratio (A1/A2) as a function of growth temperature, T_g (left axis) obtained from fitting the Se- $3d$ spectra for the Se^{2-} (A1) and $\text{Se}^{(-)}$ (A2) oxidation states. A comparison (right axes) is made with the residual resistance ratio (RRR) from electronic transport measurements. (f) Binding energy of the $3d_{5/2}$ peak for Se^{2-} obtained from fitting the data. Error bars in panels (e) and (f) is the standard deviation on the fitting parameters.

to be intrinsically linked. However, at low growth temperatures ($550 - 600^\circ\text{C}$), it appears that the strength of CDW order (T_{CDW}) approaches its maximum, whereas the crystal purity (RRR) continues to increase.

IV. X-RAY SPECTROSCOPY & DISCUSSION

To obtain information about the chemical composition of our samples, we used XPS to study core levels in $1T$ -VSe $_2$. Herein, we will mainly discuss the XPS results of the Se- $3d$ core levels for which we find a significant variation between our samples. Instead, the vanadium core levels show no noticeable variation and iodine was either not present in our samples or its concentration was below the detectable limit. These results are included in the Supplemental Material (Ref. [32]). We did not observe any sign of oxidation in the Se- $3d$ spectra which

otherwise would be in the form of SeO_2 present at ~ 59.9 eV [38] (indicated by the arrow in Fig. 4(d)). Additionally, the XAS results near the O K-edge showed a negligible amount of oxygen and all samples had identical spectra (see Ref. [32]). Therefore, we rule out the presence of oxygen or iodine as an explanation for the observed change in CDW properties.

XPS spectra for the Se- $3d$ core levels of different samples are shown in Fig. 4(a). The main feature is the doublet (labelled) with Se- $3d_{5/2} \approx 53.4$ eV and spin-orbit splitting $\Delta_{\text{so}} \approx 0.86$ eV, which corresponds to the Se^{2-} oxidation state of Se bound to V in $1T$ -VSe $_2$ [12]. An additional feature on the high energy side was also found in the region $55 - 56$ eV which is highlighted in Fig. 4(b) and shows a clear variation between samples. We find a good fit to the data using two doublets as illustrated in Fig. 4(a) for the $T_g = 630^\circ\text{C}$ sample. The binding energy (BE) of the second doublet relating to

the additional feature is $\text{Se-}3d_{5/2} \approx 54.2$ eV, which we assign to the presence of more positive oxidation states of selenium. Since it appears in our data as a single broad doublet (gaussian width ~ 2 larger than Se^{2-}), it is likely to arise from a combination of oxidation states. We label this feature $\text{Se}^{(-)}$ since its binding energy is slightly lower (i.e. more negative) than pure selenium, Se^0 which is expected at ~ 55.5 eV [38]. Such a feature could indicate the presence of partially bound or unbound Se in the form of vanadium vacancies, in-plane Se aggregates/clusters [12, 39] or Se interstitials [18] (See Fig. 1). From the fitting, the contributions of Se^{2-} and $\text{Se}^{(-)}$ states in each sample are given by the shaded areas, A1 and A2 respectively in Fig. 4(a). The ratio A1/A2 gives an indication of the relative amount of $\text{Se}^{(-)}$ oxidation states present in our samples, and is shown in Fig. 4(e) as a function of growth temperature. Comparing this ratio with the RRR from electronic measurements [right axis, Fig. 4(e)], there appears to be a correlation with the overall trend which suggests that the presence of these $\text{Se}^{(-)}$ states contribute to the impurity/defect scattering in electronic transport.

It can also be seen in Fig. 4(c) that there is a shift in binding energy of the $\text{Se-}3d$ spectra between samples. We find that this shift is significant (~ 120 meV variation), and there is an overall trend of increasing Se^{2-} binding energy for samples grown at higher temperatures as shown in Fig. 4(f). We rule out any energy shift due to local charge effects from increasing concentration of the more positive $\text{Se}^{(-)}$ oxidation states discussed previously, since there is negligible broadening of the observed Se^{2-} linewidth between samples. Such a local effect would rather be expected to contribute multiple environments, leading to the inhomogeneous broadening of the observed core level in addition to a binding energy shift. Instead, the rigid shift of the entire $\text{Se-}3d$ states is better explained by a doping effect in our samples. Specifically, an overall electron doping raises the Fermi level resulting in an apparent shift of core levels to higher binding energies with respect to our XPS energy analyzer. Therefore, we suggest that samples grown at higher temperatures are either V-rich ($\text{V}_{1+x}\text{Se}_2$) or Se-deficient (VSe_{2-x}). The binding energy shift agrees with the evolution of T_{CDW} [right axis in Fig. 4(f)], and hence we suggest that the suppression of charge density wave order in $1T\text{-VSe}_2$ could be related to effective electron doping.

To provide further insight into the composition of our samples and to help elucidate the nature of defects, we obtained the crystal stoichiometry from independent lab-based XPS measurements (non-monochromatic $\text{Al-K}\alpha$ source, $h\nu = 1486.7$ eV) and lattice parameters from powder x-ray diffraction (PXRD) described in Ref. [32]. Shown in Fig. 5 are the results for the a - and c -axis lattice parameters as a function of growth temperature together with the variation of crystal stoichiometry for comparison (top-axis). Firstly, it can be seen that the stoichiometry (Se/V ratio) of our samples varies from $\text{Se}/\text{V} = 1.98 \pm 0.10$ to 1.94 ± 0.10 with increasing growth tempera-

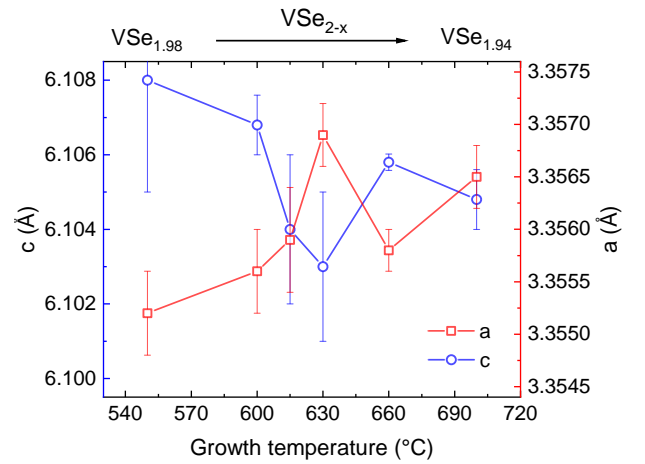


FIG. 5: Lattice parameters of $1T\text{-VSe}_2$ samples obtained from powder x-ray diffraction (PXRD). The left and right plot axes show the c - and a -axis parameters of the $\text{P}\bar{3}\text{m}1$ unit cell respectively. The top-axis labels show a comparison with the overall variation of crystal stoichiometry (Se/V ratio) obtained from laboratory XPS measurements.

ture which is consistent with the electron-doping hypothesis (either V-rich or Se-deficient). Considering these two scenarios, it is important to first examine changes in the c -axis parameter. Overall we find that it decreases with increasing growth temperature, and therefore it is unlikely that there are significant vanadium interstitials between the layers which may be expected to produce the opposite effect i.e. an *increase* in the c -axis by expanding the layer distance [40]. This is supported by our XPS and XAS data (Ref. [32]) that show no additional features which could be linked to extrinsic V species. Hence, we exclude the V-rich ($\text{V}_{1+x}\text{Se}_2$) scenario which would otherwise manifest as V interstitials in the vdW gap [22, 25]. Instead, we consider what would be the effects of Se-deficiency on the crystal structure. A study of controlled Se loss by annealing in the related compound, $1T\text{-TiSe}_2$ [41] previously showed a decrease in the c -axis related to the Ti-Se bond length, as δ increases in $\text{TiSe}_{2-\delta}$ and occurs continuously across the range 350 - 950°C. At the same time, a corresponding increase in the a -axis was observed. This trend of the a - and c -lattice parameters is very similar to what we find for $1T\text{-VSe}_2$ in Fig. 5. Therefore, we suggest that our results can be explained by an overall Se-deficiency (VSe_{2-x}) at higher growth temperatures due to increasing Se vacancies (defect B in Fig. 1). The desorption of Se at elevated temperatures is in line with previous reports [18, 24] and seems to be of greater significance above 600-700°C [42], which is consistent with our observations. As Se becomes volatile and leaves behind a vacancy, the majority is lost from the crystal. However, a small proportion may become trapped in-plane as aggregates/clusters or between layers as interstitials (defect C and E in Fig. 1 respectively). This may explain the additional $\text{Se}^{(-)}$ selenium species seen in XPS [Fig. 4(a)]. It could also be possible that

some additional Se is incorporated into the crystals due to the Se-rich environment during the growth process. This would likely occur at higher growth temperatures considering the greater energy cost to disrupt the lattice by introducing an aggregate or interstitial compared to a vacancy.

Finally, to mimic the effects of growing crystals at high temperatures, we also performed an annealing experiment to investigate the effect on the Se-3*d* core levels and valence band (VB). Here, we used a μ XPS technique with a focussed beam spot of 100 μ m in order to precisely measure the same region of the sample before and after annealing. Shown in Fig. 6 are the results which compare the pristine sample (cleaved in ultra-high vacuum, UHV), with that following heat treatment (annealing to 520°C for \sim 40 mins). Similar to Ref. [41], we expect annealing to result in Se loss from the sample, leading to a binding energy shift as the sample becomes overall electron doped. Indeed, this effect is clearly visible in Fig. 6(a) and the inset shows that the core levels are shifted by approximately 0.5 eV. Although this is much larger than the intrinsic shift in Fig. 4(c), the annealing experiments were performed in UHV ($<1 \times 10^{-9}$ mbar) as opposed to the Se-rich atmosphere during crystal growth. Given the high vapor pressure of Se (0.07 atm at 520°C), the greater loss of Se in UHV is expected. As discussed previously, the overall electron doping raises the Fermi level meaning that the core levels shift to higher binding energy. This is confirmed by analyzing the VB spectra in Fig. 6(b) where the same 0.5 eV shift is applied to the annealed sample spectrum such that the main features of the VB are overlaid. The up-shifted Fermi level position is indicated by the arrow. These results provide further evidence for the electron-doping scenario, specifically due to an overall Se-deficiency (VSe_{2-x}).

In summary, there are likely to be two major types of defects in 1*T*-VSe₂ grown by CVT; namely Se vacancies and trapped Se aggregates or interstitials. Both will contribute to the defect scattering of carriers in electronic transport and hence decrease the RRR. However, the effective binding energy shift in XPS suggests that the dominant defect type is Se vacancies as the system becomes overall electron doped. This is further supported by the Se deficiency from measurements of the crystal stoichiometry, lattice parameters and annealing experiments. We suggest that the suppression of the CDW order is caused by a deviation from stoichiometry in the form of electron doping which reduces T_{CDW} , similar to 1*T*-TiSe₂ [25]. Although the density of defects and doping level are coincidentally linked, we suggest that the CDW is mainly influenced by doping. In fact, a recent STM investigation of the local density of states in the presence of defects showed the CDW gap in 1*T*-VSe₂ to be extremely robust to disorder [43]. From our results, this is evidenced by the fact that the T_{CDW} approaches a maximum as the crystal stoichiometry becomes near 2:1 ratio at the lowest growth temperature concomitant with a saturation of the binding energy shift in XPS (doping

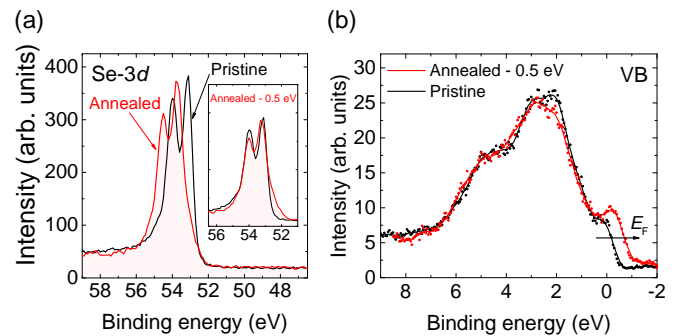


FIG. 6: Effect of annealing on core levels measured by μ XPS ($h\nu = 1486.7$ eV). (a) Se-3*d* spectra for the $T_g = 630^\circ\text{C}$ sample. A comparison is made between the pristine sample (black) after cleaving in UHV, and the effect of annealing at 520°C for \sim 40 minutes (red). The inset shows the same comparison with a shift of -0.5 eV applied to the annealed sample spectrum. (b) Valence band (VB) spectra for the pristine and annealed sample (with -0.5 eV shift applied).

level). Instead, the crystal purity (RRR) is expected to continue to increase below $T_g = 550^\circ\text{C}$ without any significant gain in T_{CDW} . We note that this is approaching the lower limit of reported growth temperatures for 1*T*-VSe₂ and other TMDs using the iodine CVT technique [23]. By decreasing the temperature further, we anticipate that the growth rate will become increasingly slow until the required growth time is impractical or there is insufficient energy for crystallization to occur.

V. CONCLUSION

From electronic transport measurements, we showed that both the CDW transition temperature, T_{CDW} and the residual resistance ratio (RRR) decreases for 1*T*-VSe₂ crystals grown at higher temperatures. This is a result of an increased density of defects, which primarily manifests as Se vacancies as a result of Se desorption from the final crystal products at elevated temperature. Therefore, we suggest 1*T*-VSe₂ becomes overall Se deficient which is confirmed by stoichiometry analysis and changes in the unit cell parameters from x-ray diffraction. This deficiency leads to an effective electron doping and a resulting up-shift in the Fermi level, which is evidenced by a rigid shift of Se-3*d* core levels to higher binding energy in XPS measurements. Although the crystal purity is reduced at higher growth temperatures (lower RRR) due to a larger density of defects, we suggest that the effective electron doping due to overall Se-deficiency is mostly responsible for the reduction in T_{CDW} . For samples with $T_g < 630^\circ\text{C}$, we see an increase in the CDW transition temperature above the typically reported value of $T_{CDW} \approx 110$ K. Based on this knowledge, we were able to optimize the chemical vapour transport method in order to produce ultra-high purity 1*T*-VSe₂ samples with near ideal stoichiometry at $T_g = 550^\circ\text{C}$ with $T_{CDW} =$

(112.7 ± 0.8) K and maximum RRR ≈ 49 .

Our work highlights the importance of carefully controlling the growth conditions of strongly correlated TMDs whose properties are sensitive to defects and deviation from stoichiometry. In addition, the growth of high purity TMD materials is imperative for understanding both the bulk behaviour of these compounds and to provide a suitable source for exfoliation of monolayers and the preparation of van der Waals heterostructures.

Acknowledgements

We thank the Elettra synchrotron for access to the BEAR beamline (proposal no. 20180358) and the BEAR

staff for assistance during measurements including S. Nannarone and N. Mahne for helpful discussions. Extensive technical support from P. Jones at the University of Bath is gratefully appreciated. We would like to thank S. Cross and S. Friedemann for insightful discussions and sharing preliminary data. We thank G. Balakrishnan for sharing unpublished information with regards to Ref. [35]. The authors acknowledge funding and support from the EPSRC Centre for Doctoral Training in Condensed Matter Physics (CDT-CMP), Grant No. EP/L015544/1. Finally, we acknowledge the Bristol NanoESCA Facility (EPSRC Strategic Equipment Grant No. EP/K035746/1 and EP/M000605/1).

-
- [1] J. A. Wilson, F. J. Di Salvo, and S. Mahajan, Charge-density waves and superlattices in the metallic layered transition metal dichalcogenides, *Adv. Phys.* **24**, 117 (1975).
- [2] K. Rossnagel, On the origin of charge-density waves in select layered transition-metal dichalcogenides, *J. Phys. Condes. Mat.* **23**, 213001 (2011).
- [3] K. Tsutsumi, X-ray-diffraction study of the periodic lattice distortion associated with a charge-density wave in 1T-VSe₂, *Phys. Rev. B* **26**, 5756 (1982).
- [4] D. J. Eaglesham, R. L. Withers, and D. M. Bird, Charge-density wave transitions in 1T-VSe₂, *J. Phys. C* **19**, 359 (1986).
- [5] A. H. Thompson, and B. G. Silbernagel, Correlated magnetic and transport properties in the charge-density-wave states of VSe₂, *Phys. Rev. B* **19**, 3420 (1979).
- [6] K. Terashima, T. Sato, H. Komatsu, and T. Takahashi N. Maeda and K. Hayashi, Charge-density wave transition of 1T-VSe₂ studied by angle-resolved photoemission spectroscopy, *Phys. Rev. B* **68**, 155108 (2003).
- [7] V. N. Strocov, M. Shi, M. Kobayashi, C. Monney, X. Wang, J. Krempasky, T. Schmitt, L. Patthey, H. Berger, and P. Blaha, Three-dimensional electron realm in VSe₂ by soft-x-ray photoelectron spectroscopy: origin of charge-density waves, *Phys. Rev. Lett.* **109**, 086401 (2012).
- [8] Á. Pásztor, A. Scarfato, C. Barreateau, E. Giannini and C. Renner, Dimensional crossover of the charge density wave transition in thin exfoliated VSe₂, *2D. Mat.* **4**, 041005 (2017).
- [9] J. Yang, W. Wang, Y. Liu, H. Du, W. Ning, G. Zheng, C. Jin, Y. Han, N. Wang, Z. Yang, M. Tian, and Y. Zhang, Thickness dependence of the charge-density-wave transition temperature in VSe₂, *Appl. Phys. Lett.* **105**, 063109 (2014).
- [10] Y. Ma, Y. Dai, M. Guo, C. Niu, Y. Zhu, and B. Huang, Evidence of the Existence of Magnetism in Pristine VX₂ Monolayers (X = S, Se) and Their Strain-Induced Tunable Magnetic Properties, *ACS. Nano.* **6**, 1695 (2012).
- [11] M. Bonilla, S. Kolekar, Y. Ma, H. C. Diaz, V. Kalappattil, R. Das, T. Eggers, H. R. Gutierrez, M. H. Phan and M. Batzill, Strong room-temperature ferromagnetism in VSe₂ monolayers on van der Waals substrates, *Nat. Nano.* **13**, 289 (2018).
- [12] Z.-L. Liu, X. Wu, Y. Shao, J. Qi, Y. Cao, L. Huang, C. Liu, J.-O. Wang, Q. Zheng, Z.-L. Zhu, K. Ibrahim, Y.-L. Wang and H.-J. Gao, Epitaxially grown monolayer VSe₂: an air-stable magnetic two-dimensional material with low work function at edges, *Sci. Bull.* **63**, 419 (2018).
- [13] J. Feng, D. Biswas, A. Rajan, M. D. Watson, F. Mazzola, O. J. Clark, K. Underwood, I. Marković, M. McLaren, A. Hunter, D. M. Burn, L. B. Duffy, S. Barua, G. Balakrishnan, F. Bertran, P. Le Fèvre, T. K. Kim, G. van der Laan, T. Hesjedal, P. Wahl, and P. D. C. King, Electronic Structure and Enhanced Charge-Density Wave Order of Monolayer VSe₂, *Nano. Lett.* **18**, 4493 (2018).
- [14] P. Chen, W. W. Pai, Y. -H. Chan, V. Madhavan, M. Y. Chou, S. -K. Mo, A. -V Federov, and T. -C. Chiang, Unique Gap Structure and Symmetry of the Charge Density Wave in Single-Layer 1T-VSe₂, *Phys. Rev. Lett.* **121**, 196402 (2018).
- [15] H. Wang, X. Huang, J. Lin, J. Cui, Y. Chen, C. Zhu, F. Liu, Q. Zeng, J. Zhou, P. Yu, X. Wang, H. He, S. H. Tsang, W. Gao, K. Suenaga, F. Ma, C. Yang, L. Lu, T. Yu, E. H. T. Teo, G. Liu and Z. Liu High-quality monolayer superconductor NbSe₂ grown by chemical vapour deposition, *Nat. Comms.* **8**, 394 (2017).
- [16] W. Fu, Y. Chen, J. Lin, X. Wang, Q. Zeng, J. Zhou, L. Zheng, H. Wang, YHe, H. He, Q. Fu, K. Suenaga, T. Yu, and Z. Liu, Controlled Synthesis of Atomically Thin 1T-TaS₂ for Tunable Charge Density Wave Phase Transitions, *Chem. Mater.* **28**, 7613 (2016).
- [17] Q. Yu, L. A. Jauregui, W. Wu, R. Colby, J. Tian, Z. Su, H. Cao, Z. Liu, D. Pandey, D. Wei, T. F. Chung, P. Peng, N. P. Guisinger, E. A. Stach, J. Bao, S. S. Pei and Y. P. Chen, Control and characterization of individual grains and grain boundaries in graphene grown by chemical vapour deposition, *Nat. Mat.* **10**, 443 (2011).
- [18] J. P. Peng, J. Q. Guan, H. M. Zhang, C. Li. Song, L. Wang, K. He, Q. K. Xue, X. C. Ma, Molecular beam epitaxy growth and scanning tunneling microscopy study of TiSe₂ ultrathin films, *Phys. Rev. B* **91**, 121113(R) (2015).
- [19] D. Zhang, J. Ha, H. Baek, Y.-H. Chan, F. D. Natterer, A. F. Myers, J. D. Schumacher, W. G. Cullen, A. V. Davydov, Y. Kuk, M. Y. Chou, N. B. Zhitenev, and J.

- A. Strocio, Strain engineering a $4a \times \sqrt{3}a$ charge-density-wave phase in transition metal dichalcogenide 1T-VSe₂, *Phys. Rev. Mater.* **1**, 024005 (2017).
- [20] A. Castellanos-Gomez, M. Buscema, R. Molenaar, V. Singh, L. Janssen, H. S. J. van der Zant, and G. A. Steele, Deterministic transfer of two-dimensional materials by all-dry viscoelastic stamping, *2D. Mater.* **1**, 011002 (2014).
- [21] K. Hayashi and M. Nakahira, Stability and The Equilibrium Selenium Vapor Pressure of the 1T-VSe₂ Phase, *J. Solid. State. Chem.* **24**, 153 (1978).
- [22] F. J. Di Salvo and J. V. Waszczak, Magnetic studies of VSe₂, *Phys. Rev. B.* **23**, 457 (1981).
- [23] F. Levy and Y. Froidevaux, Structural and electrical properties of layered transition metal selenides V_xTi_{1-x}Se₂ and Ta_xTi_{1-x}Se₂, *J. Phys. C: Solid. State. Phys.* **12**, 473 (1979).
- [24] B. Hildebrand, C. Didiot, A. M. Novello, G. Monney, A. Scarfato, A. Ubaldini, H. Berger, D. R. Bowler, C. Renner, and P. Aebi, Doping nature of native defects in 1T-TiSe₂, *Phys. Rev. Lett.* **112**, 197001 (2014).
- [25] F. J. Di Salvo, D. E. Moncton and J. V. Waszczak, Electronic properties and superlattice formation in the semimetal TiSe₂, *Phys. Rev. B.* **14**, 4321 (1976).
- [26] C. S. Yadav, and A. K. Rastogi, Electronic transport and specific heat of 1T-VSe₂, *Solid. State. Comms.* **150**, 648 (2010).
- [27] A. Toriumi and S. Tanaka, Galvanomagnetic properties of 1T-VSe₂, *Physica. B+C.* **105**, 141 (1981).
- [28] H. Hedayat, C. J. Sayers, D. Bugini, C. Dallera, D. Wolverson, T. Batten, S. Karbassi, S. Friedemann, G. Cerullo, J. van Wezel, S. R. Clark, E. Carpena, and E. Da Como, Excitonic and lattice contributions to the charge density wave in 1T-TiSe₂ revealed by a phonon bottleneck, *Phys. Rev. Research.* **1**, 023029 (2019).
- [29] H. P. B. Rimmington and A. A. Balchin, The growth by iodine vapour transport techniques and the crystal structures of layer compounds in the series TiS_xSe_{2-x}, TiS_xTe_{2-x}, *J. Crys. Growth.* **21**, 171 (1974).
- [30] S. Nannarone, F. Borgatti, A. DeLuisa, B. P. Doyle, G. C. Gazzadi, A. Giglia, P. Finetti, N. Mahne, L. Pasquali, M. Pedio, G. Selvaggi, G. Naletto, M. G. Pelizzo, and G. Tondello, The BEAR Beamline at Elettra, *AIP. Conf. Proc.* **705**, 450 (2004).
- [31] L. Pasquali, A. De Luisa, and S. Nannarone, The UHV Experimental Chamber For Optical Measurements (Reflectivity and Absorption) and Angle Resolved Photoemission of the BEAR Beamline at Elettra, *AIP. Conf. Proc.* **705**, 1142 (2004).
- [32] See Supplemental Material at <http://link.aps.org/> for a summary of the 1T-VSe₂ sample properties, details of PXRD measurements, methods of determining the CDW phase transition temperature, T_{CDW} and x-ray spectroscopy (XPS and XAS) of vanadium and iodine core levels.
- [33] C. F. van Bruggen, and C. Haas, Magnetic susceptibility and electrical properties of VSe₂ single crystals, *Solid. State. Comms.* **20**, 251 (1976).
- [34] M. Bayard and M. J. Sienko, Anomalous electrical and magnetic properties of vanadium diselenide, *J. Solid. State. Chem.* **19**, 325 (1976).
- [35] S. Barua, M. C. Hatnean, M. R. Lees and G. Balakrishnan, Signatures of the Kondo effect in VSe₂, *Sci. Rep.* **7**, 10964 (2017).
- [36] M. Naito and S. Tanaka, Electrical Transport Properties in 2H-NbS₂, -NbSe₂, -TaS₂ and -TaSe₂, *J. Phys. Soc. Jpn.* **51**, 219 (2017).
- [37] K. Cho, M. Kończykowski, S. Teknowijoyo, M. A. Tanatar, J. Guss, P. B. Gartin, J. M. Wilde, A. Kreyssig, R. J. McQueeney, A. I. Goldman, V. Mishra, P. J. Hirschfeld and R. Prozorov, Using controlled disorder to probe the interplay between charge order and superconductivity in NbSe₂, *Nat. Comms.* **9**, 2796 (2018).
- [38] M. Shenasa, S. Sainkar and D. Lichtman, XPS Study of Some Selected Selenium Compounds, *J. Electron. Spec. Relat. Phenom.* **40**, 329 (1986).
- [39] X. Chia, A. Ambrosi, P. Lazar, Z. Sofer, and M. Pumera, Electrocatalysis of layered Group 5 metallic transition metal dichalcogenides (MX₂, M = V, Nb, and Ta; X = S, Se, and Te), *J. Mater. Chem. A.* **4**, 14241 (2016).
- [40] E. Morosan, H. W. Zandbergen, B. S. Dennis, J. W. G. Bos, Y. Onose, T. Klimczuk, A. P. Ramirez, N. P. Ong and R. J. Cava, Superconductivity in Cu_xTiSe₂, *Nat. Phys.* **2**, 544 (2006).
- [41] S. H. Huang, G. J. Shu, Woei Wu Pai, H. L. Liu, and F. C. Chou, Tunable Se vacancy defects and the unconventional charge density wave in 1T-TiSe_{2-δ}, *Phys. Rev. B.* **95**, 045310 (2017).
- [42] L. N. Zelenina, T. P. Chusova and A. N. Titov, Thermodynamic properties of titanium selenides with variable composition TiSe₂-TiSe_{1.80}, *Russ. Chem. Bull.* **60**, 581 (2011).
- [43] W. Jolie, T. Knispel, N. Ehlen, K. Nikonov, C. Busse, A. Grüneis, and T. Michely, Charge density wave phase of VSe₂ revisited, *Phys. Rev. B.* **99**, 115417 (2019).